Materials Science & Engineering A 718 (2018) 492–498

Contents lists available at ScienceDirect

Materials Science & Engineering A

journal homepage: www.elsevier.com/locate/msea

Preliminary creep testing of the alumina-forming austenitic stainless steel Fe-20Cr-30Ni-2Nb-5Al

Ian Baker*, Natalie Afonina[1], Zhangwei Wang[2], Margaret Wu

Thayer School of Engineering, Dartmouth College, Hanover, NH 03755, USA

ARTICLE INFO

Keywords:
Creep
AFA steel
Precipitation
Tensile testing
Microstructural characterization

ABSTRACT

The alumina-forming austenitic stainless steel Fe-20Cr-30Ni-2 Nb-5Al was given a solutionizing anneal at 1250 °C followed by anneals at 800 °C for 0, 2.4, 24, 240 h to produce B2 (ordered b.c.c.) and Laves phase precipitates of different sizes with different extents of grain boundary coverage. Both tensile tests and constant-stress (43 MPa) creep tests were performed on the heat-treated materials and on the as-cast alloy at 760 °C. The precipitates grew during the creep testing. In addition, $L1_2$ (ordered f.c.c.) precipitates nucleated and grew during the creep testing to similar particle sizes after 500 h independent of the prior heat treatment at 800 °C. The specimens given the shortest heat treatment of 2.4 h, which had the smallest initial particle sizes, showed both the highest yield strength and the smallest creep strain after 500 h. The extent of grain boundary coverage by precipitates did not appear to affect the creep rates. No grain boundary cracking or precipitate cracking was found in the heat-treated specimens after creep testing, but the as-cast material failed around 600 h.

1. Introduction

In order for power plants to be more efficient they need to run at higher temperature: an operating temperature increase from 600 °C to 800 °C would increase the efficiency from < 40% to > 50%, and reduce CO_2 emissions by 40–50% (Smith and Shoemaker, 2004). This requires materials that are strong enough, can withstand an environment that may contain impurities in addition to steam, display good oxidation and corrosion resistance and are economically viable [27]. Affordable materials that can satisfy these requirements may also likely find use in supercritical CO_2 cycles and in tubing for concentrated thermal solar power.

The martensitic/ferritic alloys that are currently used in power plants are limited to operating temperatures ≤ 600 °C [26]. Nickel-based superalloys, some titanium alloys, and, possibly, oxide-dispersion strengthened ferritic alloys [15,16, 17] can satisfy the strength and, at least for nickel-based alloys, the oxidation and corrosion requirements at elevated temperatures. Unfortunately, these materials are too expensive except for use in specialized applications [18].

Some recent efforts in this area have focused on devising new austenitic steels strengthened with Laves phases [13,18,19,28,29,31], whose purpose is to provide a “grain boundary (GB) precipitation strengthening mechanism” [20,21]. The addition of aluminum can be used to improve oxidation resistance in these alloys [28,29,3,30,4,5]. Such alumina-forming austenitic (AFA) stainless steels have shown promise to decrease our reliance on expensive nickel-based alloys for aggressive conditions in energy production and chemical processing environments [7]. AFAs use alumina instead of chromia as a protective oxide scale for high corrosion resistance since it is known to offer even better protection at high temperatures [10,12]. AFA stainless steels were in development as early as the 1970s [14] and, more recently, a new family of AFAs has been under development at the Oak Ridge National Laboratory, ORNL [28,29,3,30,31,33,4,6,7]. In the newer grades of AFAs, B2-structured (ordered b.c.c.) NiAl and Laves phase precipitates are present on both the GBs and in the austenitic matrix, while MC precipitates or $L1_2$-structured (ordered f.c.c.) Ni_3Al precipitates, which are present only in the matrix, are used to increase the creep strength [31,33,7].

A wide variety of creep strengths can be obtained with relatively small changes in alloying elements, and phases that are beneficial in some AFAs appear to cause decreased creep strength in others. There are three grades of AFAs that have been investigated by the ORNL group based on their nickel content (in wt%), *viz.*, 12Ni, 20–25Ni and 32Ni. The 12Ni grade alloys substitute Mn for some of the Ni both to stabilize the austenite relative to the deleterious δ–Fe phase and to lower the cost. Unfortunately, this grade has been shown to have

* Corresponding author.
E-mail address: Ian.Baker@Dartmouth.edu (I. Baker).
[1] Current address: Uber Technologies Inc., 555 Market St, 17th Floor, San Francisco, CA 94105.
[2] Current address: Max-Planck-Institut für Eisenforschung GmbH, Max-Planck-Straße 1, D-40237 Düsseldorf, Germany.

https://doi.org/10.1016/j.msea.2018.01.090
Received 26 October 2017; Received in revised form 12 January 2018; Accepted 22 January 2018
Available online 03 February 2018
0921-5093/

relatively poor creep resistance although the reason for the decreased creep strength is poorly understood [33,7]. In 20–25 Ni grade alloys it has been found that the total weight fraction of carbide phases is important. For example, in a 20–25Ni grade alloy with 2.53 wt% Nb and 0.2 wt% C there was little MC supersaturation and it showed poor creep resistance compared to 25Ni grade alloys with 1 wt% Nb and 0.1 wt% C. It is believed that the 2.53 wt% Nb alloy showed poorer creep strength because the 2.53 wt% Nb addition decreased the supersaturation of MC carbides [7]. The 1 wt% Nb and 0.1 wt% C additions have been shown to be the optimal amounts for MC carbide strengthening in other studies of AFAs as well [32,6]. While increasing the Nb content from 1 wt% to 2.5 wt% seemed to have a detrimental role on the creep strength for a 25Ni alloy, in the 32Ni grade alloys with 3.3 wt % Nb superior creep strength has been observed at 650 °C a feature that appears to be due to strengthening from $L1_2$ Ni_3Al precipitates, producing a creep strength almost five times greater than the best carbide-strengthened 20–25 Ni alloy. While the $L1_2$ – structured Ni_3Al precipitates improved the creep properties of the 32Ni alloy, at 650 °C it is believed that the metastable $L1_2$ Ni_3Al caused the decreased rupture time observed in a 25Ni-4Al-1 Nb alloy with increased C content compared to a 25Ni-3Al-1 Nb alloy. Although the creep strength was promising there was a tradeoff with significantly reduced creep elongation in the 32Ni grade alloy, which is thought to be due to σ-phase formation. At 750 °C the 32Ni alloy creep results were comparable to those of both the 20–25Ni and 12Ni alloy grades [7].

Similarly, Dong et al. [8] studied the creep behavior of Fe-19.95Ni-14.19Cr-2.25Al-2.26Mo-1.95Mn-0.15Si-0.01B (wt%) at 700 °C and 150 MPa and found that an alloy with 0.86% Nb and 0.07% C had poor creep behavior due to the relatively coarse (100 nm) NbC, whereas a similar alloy with a lower carbon content (0.04%) had much smaller carbides (10 nm) and much improved creep properties. An alloy with the same carbon content but lower Nb (0.5%) and the addition of 0.2% V had even better creep properties due to the formation of (Nb, V)C. Both Laves phase and NiAl were found to be present after the creep testing, but Dong et al. [8] questioned whether they contributed to the creep strength.

32Ni grade alloys with decreased chromium content (14 wt% versus 19 wt%) and additional alloying elements such as Zr and Ti have less σ-phase formation and improved creep properties. Indeed, a Zr, Ti alloyed 32Ni alloy with additions of carbon and boron was shown to have a creep-rupture life that exceeded that of the commercially-available Fe-base alloy A286 by an order of magnitude [34]. The addition of boron to a 32Ni grade alloy increased the resistance to creep deformation, but it is unclear why [34]. It is worth noting that solutionizing anneals of the complex ORNL alloys still leave substantial volume fractions of the Laves phase in the material [34,7].

For many of the AFA alloys that were also tensile tested, the creep and elevated temperature tensile properties did not correlate well. For example, in the 20–25 Ni grade alloys while B2-NiAl and Laves precipitation improves tensile properties, MC carbides appear to show a stronger influence on the creep strength [33,7]. The ORNL group also questioned whether the Laves phase even had any significant influence on the creep strength [2]. The lower tensile strength they observed in these alloys at 1023 K compared to room temperature appeared to be due to the softening of the B2 NiAl phase which produces significant strengthening at room temperature. This lack of correlation between the elevated temperature yield strength and the creep life is well illustrated in the data presented by Dong et al. [8], see Table 1, although the strain hardening exponent, *n*, did show roughly the same trend as the creep life.

In earlier work, we studied the precipitation kinetics, precipitate/matrix orientation relationships and room temperature mechanical properties of the AFA steel Fe-20Cr-30Ni-2 Nb-5Al after various thermo-mechanical treatments [22,25]. In this paper we examine the effects of different heat treatments at 800 °C on both the tensile test behavior and creep rate at 760 °C. At the latter temperature the alloy contains B2, Laves phase and $L1_2$ precipitates.

Table 1
Yield strength (YS), ultimate tensile strength (UTS), elongation to failure (ε_f) and strain hardening exponent, *n*, of Fe-19.95Ni-14.19Cr-2.25Al-2.26Mo-1.95Mn-0.15Si-0.01B (wt %) strained under tension at 5×10^{-4} s^{-1} at 750 °C, and corresponding creep life at 973 K and 150 MPa for various alloying additions. After [8].

Alloying additions	YS, MPa	UTS, MPa	ε_f (%)	*n*	Creep Life (h)
.86 Nb, 0.07 C	229	272	50	0.11	164
0.86 Nb, 0.04 C	175	315	44	0.38	1002
0.50 Nb, 0.04 C, 0.20 V	160	330	52	0.48	1537

Table 2
Comparison of the desired and measured elemental compositions obtained by LECO combustion analysis and X-ray fluorescence.

Element Analyzed	Desired (wt%)	Analyzed (wt%)
Nickel	31.88	31.9
Chromium	18.83	18.98
Niobium	3.36	3.34
Aluminum	2.44	2.48
Carbon	0.00	0.02
Cobalt	0.00	0.01
Copper	0.00	< 0.01
Manganese	0.00	< 0.01
Molybdenum	0.00	0.01
Phosphorus	0.00	< 0.005
Silicon	0.00	< 0.01
Sulfur	0.00	< 0.001

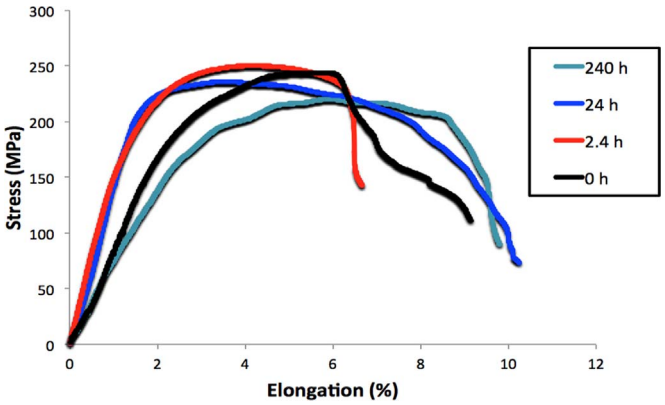

Fig. 1. Typical stress-strain curves for Fe-20Cr-30Ni-2 Nb-5Al tensile tested at 760 °C solutionized at 1250 °C for 24 h followed by the heat-treatment at 800 °C for the times indicated.

Table 3
Comparison of yield strength (YS) and elongation (ε_f) from tensile tests at room temperature (RT) and 760 °C. The values are from three tests at each condition. The room temperature data are from [22].

Aging Time (h)	YS (MPa) RT	ε_f (%) RT	YS (MPa) 760 °C	ε_f (%)760 °C
0	205	52	188	7.7
2.4	322	37	225	5.7
24	362	29	202	8.9
240	351	28	166	9.6
1325	383	19	N/A	N/A

2. Experimental

Split-cast vacuum induction was used to cast the Fe-20Cr-30Ni-2 Nb-5Al (at%) into 8 kg tapered ingots at Carpenter Technology Corporation (Wyomissing, PA), courtesy of Michael Schmidt. The ingots were press forged into rectangular bars of dimensions

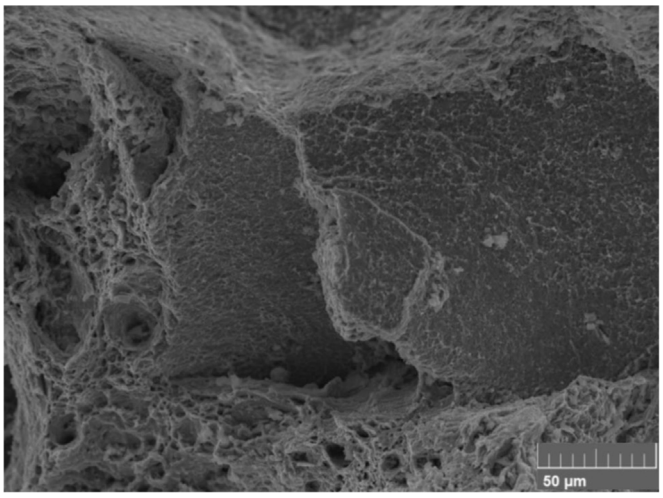

Fig. 2. BSE image of fracture surface for Fe-20Cr-30Ni-2 Nb-5Al aged for 24 h at 800 °C for 240 h and tensile tested at 760 °C.

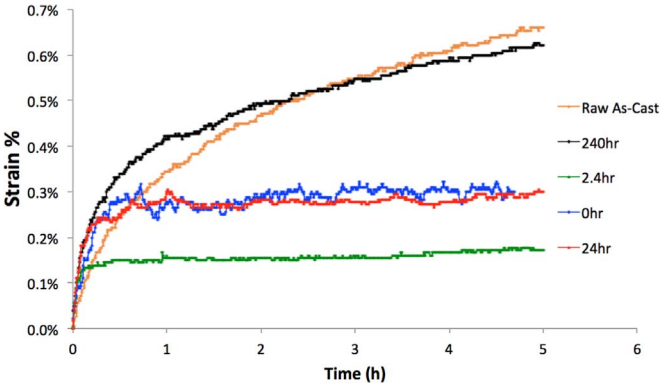

Fig. 3. Initial creep curves for a constant stress of 43 MPa at 760 °C for Fe-20Cr-30Ni-2 Nb-5Al solutionized at 1250 °C for 24 h followed by the heat-treatment at 800 °C for the times indicated.

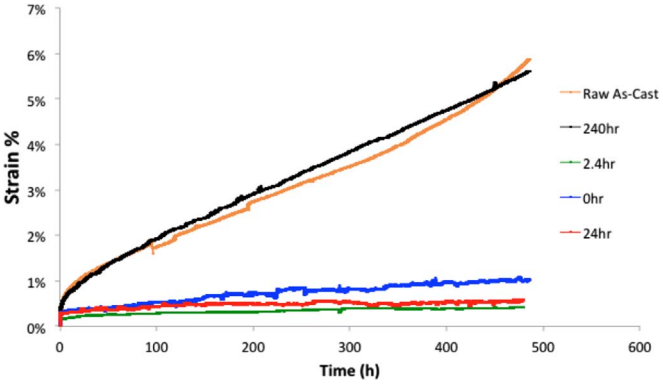

Fig. 4. Creep curves for Fe-20Cr-30Ni-2 Nb-5Al given different heat treatments at 800 °C. Applied constant stress of 43 MPa at 760 °C. All tests were terminated at ~500 h.

16 × 19 × 61 mm. The chemical composition of the alloy was analyzed by LECO combustion analysis and X-ray fluorescence. Table 2 shows the desired and analyzed elemental compositions.

An anneal of 24 h at 1250 °C under vacuum followed by quenching in water was used to solutionize the alloy. To develop different precipitation distributions, specimens were heat treated under argon at 800 °C for 0, 2.4, 24 or 240 h followed by quenching into water. These are the same heat treatments used in our previous studies [22,25].

Flat T-bone specimens with a gauge cross-section of 1 mm × 2 mm thick, with a gauge length of 15 mm were used for tensile tests. Specimens were polished using successively finer silicon carbide abrasive paper up to 1200-grit, then finished with 0.3 μm alumina. Tensile tests were conducted at 760 °C at an initial strain rate of $5 \times 10^{-4}\ s^{-1}$. Up to five tensile tests were performed for each heat treatment. True stress and true strain curves were calculated from the load-displacement data, while elongations were measured directly from the specimens.

Tensile creep test specimens were milled with a gauge cross-section of 3 × 3 mm with a gauge length of 20 mm. Creep tests were performed at 760 °C at a stress of 43 MPa on a home-built constant-stress creep jig. Details of the creep jig, which was based on a design by Garofalo, Richmond and Domis [9], can be found in Afonina [1]. The elongation was recorded as a function of time and plotted as creep strain versus time. A creep test was performed for each heat treatment noted above and for the as-cast alloy.

Specimens were examined using back-scattered electron (BSE) imaging before and after tensile testing and creep testing using a Tescan Vega3 scanning electron microscope (SEM) outfitted with a Bruker Quantax Energy-dispersive X-ray Spectrometer (EDS) operated at 15 keV. BSE imaging enables the NiAl and Laves phase precipitates to be distinguished simply based on atomic number contrast [22]. Preparation for SEM examination involved mounting the specimens in phenolic resin and polishing on 1200-grit SiC paper, followed by polishing with 0.3 μm and then 0.05 μm alumina powder. Specimens were given a final polish for ~3 h in a vibratory polisher using 60 nm colloidal silica polishing suspension.

For quantitative analysis of the NiAl and Laves phase precipitates, particle density and average particle diameter were analyzed using ImageJ image processing software. BSE images were taken at 4000 × and pre-processed to optimize uniformity of illumination and contrast in the input images. This step consisted of reducing artifacts generated by the acquisition system, contrast enhancement, despeckling and setting the threshold at a level that allows for differentiation between the lighter, brighter-contrasted Laves phase particles and the darker-contrasted NiAl precipitates. After the proper threshold was established, images were processed with outlier filters. Particle diameter and density were calculated.

Crept specimens were examined using a FEI Tecnai F20 field emission gun transmission electron microscope (TEM) operated at 200 kV. For TEM examination, 100 μm thick, 3 mm diameter discs were electrolytically thinned in a polishing electrolyte solution consisting of 20% nitric acid and 10% butoxyethanol in methanol in the temperature range of −20 to −25 °C using a Struers TenuPol-5 at a voltage of 11 V and a current of ~50 mA. After electropolishing, the samples were rinsed three times with ethanol. The size and number density per unit area of the $L1_2$ particles after creep testing were determined from bright field images from the resulting thin foils using Image J. The volume fraction of the $L1_2$ particles was calculated from the particle density per unit area assuming a foil thickness of 100 nm.

3. Results

Fig. 1 shows typical stress curves for tensile tests at 760 °C for each heat treatment. None of the specimens showed work-hardening after yielding. Table 3 shows the average yield strength and elongation to failure at 760 °C from three tensile tests for each heat treatment. Also shown are previously performed room temperature tensile test results after the same heat treatments [22].

At room temperature, the solutionized alloy was far weaker than any of the heat-treated specimens. For the heat treated specimens, the yield strength increased with increasing particle size and volume fraction of particles, both of which increased with increasing annealing time. In contrast, at 760 °C the heat treatment that produced the finest particle size (2.4 h) produced the largest yield strength. As the particle size increased with increasing annealing time the yield strength

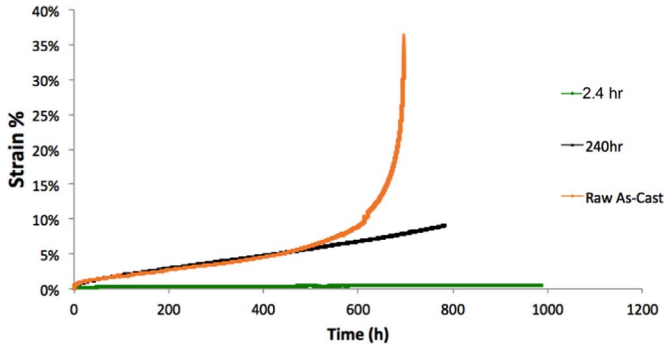

Fig. 5. Creep curves for Fe-20Cr-30Ni-2 Nb-5Al in both the as-cast condition and heat treated at either 2.4 h or 240 h at 800 °C. Applied constant stress of 43 MPa at 760 °C. The as-cast material failed while the two heat-treated specimens were terminated.

decreased. Interestingly, the specimens given the longest anneal (240 h) were weaker than the specimens that were simply solutionized, that is, the solutes present produced greater strengthening than the large particles.

At room temperature, the elongation to failure decreased with increasing annealing time. This was related to the feature that the grain boundary coverage of brittle NiAl and Laves phase particles increased with increasing annealing time until after 240 h the grain boundaries were 77% covered in particles. In contrast, while the grain boundaries had the same coverage as in the low temperature tests, for the 760 °C tests the elongation showed no correlation with the grain boundary coverage by precipitates. The elongations to failure at 760 °C where all significantly less than at room temperature. Broadly, the elongation to failure decreased as the yield strength increased at 760 °C.

The fracture surfaces after all the high temperature tests were largely the same. Fig. 2 shows a typical fracture surface, which shows regions of dimple-type rupture and regions that suggests fracture along or near the grain boundary.

Fig. 3 shows the initial 5 h of the creep curves for the Fe-20Cr-30Ni-2 Nb-5Al in the as-cast condition and after the solutionizing anneal followed by aging at 0, 2.4, 24 or 240 h at 800 °C. There are a number of interesting differences present in the creep curves. The specimen that shows the highest yield strength at 760 °C (2.4 h anneal) shows the lowest primary creep strain. The specimens that show the next largest yield strengths (0 h, 24 h) show almost twice the strain in primary creep, while the specimen with the lowest yield strength (240 h) shows

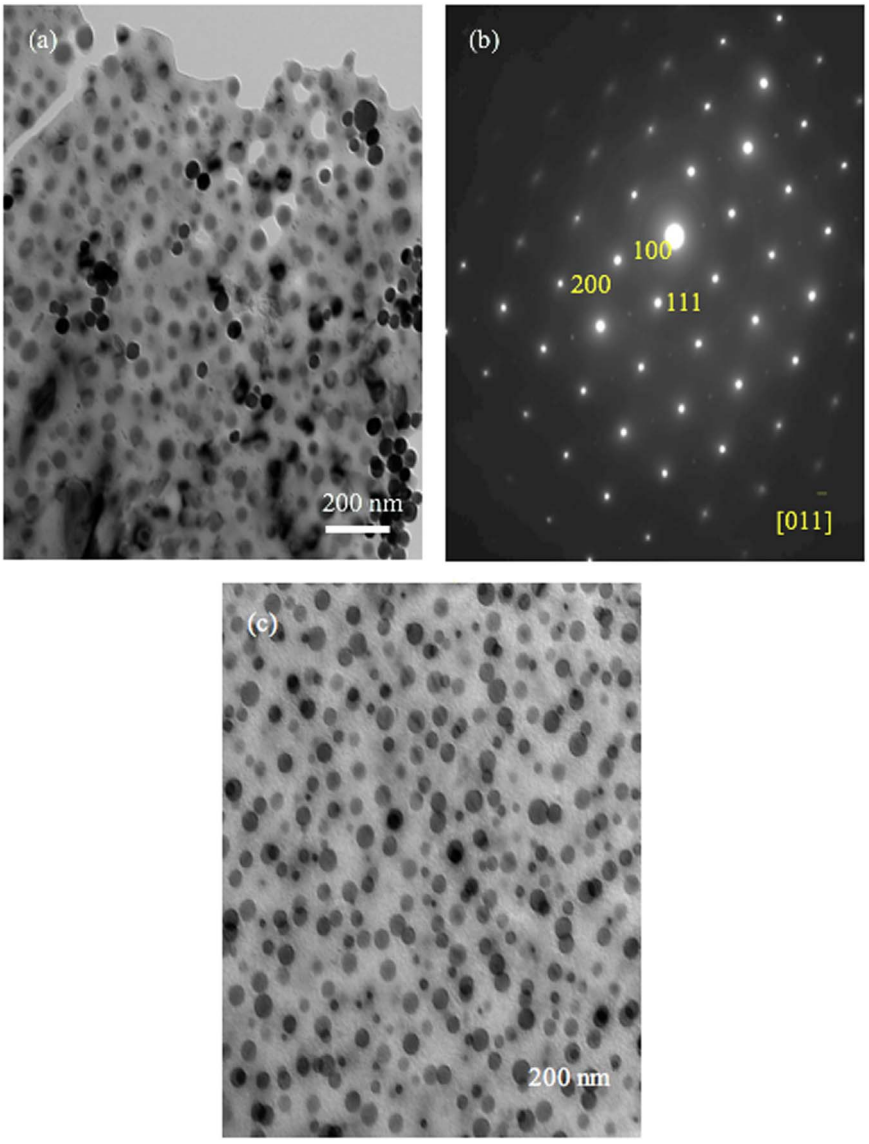

Fig. 6. Bright field TEM images of $L1_2$ precipitates in Fe-20Cr-30Ni-2 Nb-5Al solutionized at 1250 °C for 24 h and heat treated at 800 °C for (a) 0 h and (c) 2.4 h, and crept for 500 h. The SAD pattern (b), which is from the area shown in (a), shows the presence of superlattice reflections, e.g. 100.

Table 4
$L1_2$ precipitate diameter and volume fraction after creep for 500 h for different annealing times at 800 °C.

Annealing time at 800 °C (h)	Precipitate Diameter (nm)	Volume Fraction (%)
0	43 ± 15	40
2.4	44 ± 14	34
24	53 ± 14	52
240	54 ± 3	56

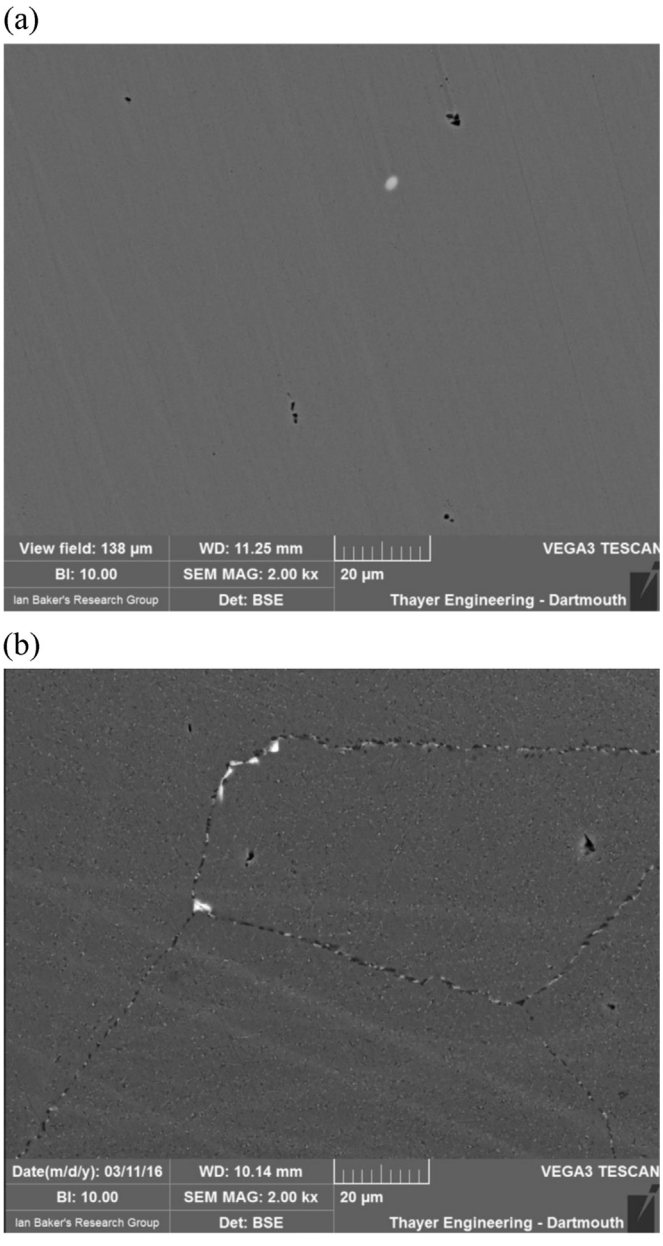

Fig. 7. BSE images of Fe-20Cr-30Ni-2 Nb-5Al solutionized at 1250 °C for 24 h (a) before and (b) after creep testing for 500 h. Note the lack of precipitates before creep testing, and the (dark) NiAl and (light) Laves phase precipitates after creep.

a substantially larger primary creep strain and primary creep continues for a longer time.

Fig. 4 shows the creep curves to 500 h for all the above specimens. It is evident that the different Laves phase and NiAl precipitate structures have a substantial affect on the creep behavior. The 2.4 h- and 24 h-annealed specimens show similar creep rates (8.8×10^{-10} s^{-1} and

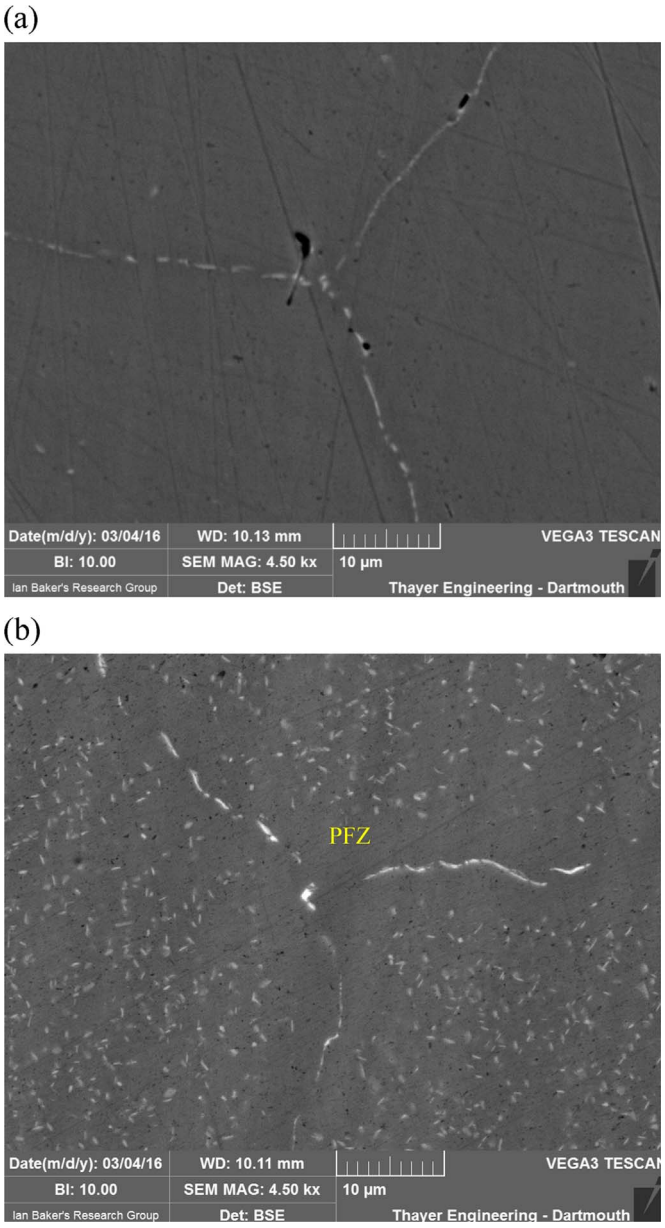

Fig. 8. BSE images of Fe-20Cr-30Ni-2 Nb-5Al solutionized at 1250 °C for 24 h and annealed for 24 h at 800 °C (a) before and (b) after creep testing for 500 h. After creep testing the precipitates are larger and a precipitate free zone (PFZ) has formed along the grain boundaries. The NiAl precipitates are dark and the Laves phase precipitates are light.

1.1×10^{-9} s^{-1}, respectively) in the secondary creep regime with the larger creep strain after 500 h present in the 24 h annealed specimen arising from the large strain acquired in primary creep. The creep rate (3.5×10^{-9} s^{-1}) of the specimen that was simply fully solutionized (0 h) is higher than the two specimens containing fine precipitates, while the 240 h annealed sample has a creep rate (3.2×10^{-8} s^{-1}) more than an order of magnitude higher than any of the three samples noted previously. In fact, the creep rate of the 240 h annealed specimen is very similar to that of the as-cast alloy. The creep tests were terminated after 500 h in order that the resulting microstructures could be examined.

Fig. 5 shows the results of additional creep tests that were performed on the two heat-treated specimens that showed the lowest and highest creep rates as shown in Fig. 4 and on the as-cast specimen. Both the heat-treated specimens continued to creep at the same rate at the longer creep times. However, surprisingly, the as-cast specimen that

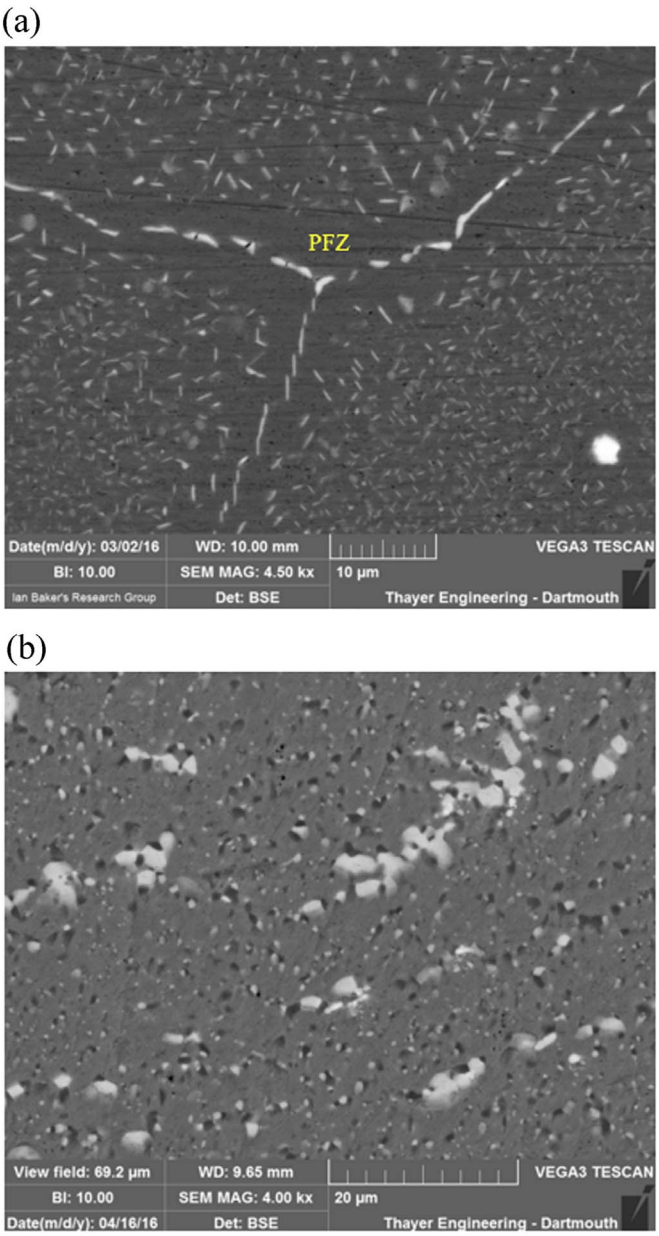

Fig. 9. BSE images of Fe-20Cr-30Ni-2 Nb-5Al solutionized at 1250 °C for 24 h and annealed for 240 h at 800 °C (a) before and (b) after creep testing for 500 h. Before creep testing a precipitate free zone (PFZ) is present along the grain boundaries. After creep testing the precipitates are larger. The NiAl precipitates are dark and the Laves phase precipitates are light.

Table 5
Diameter of Laves phase and NiAl precipitates and particle density before and after creep testing for specimens given different aging times at 800 °C and crept for 500 h at 760 °C.

	Average Particle Diameter (nm)					
	Laves		NiAl		Particle Density (particles/μm^2)	
Aging time (h)	Pre-creep	Post-creep	Pre-creep	Post-creep	Pre-creep	Post-creep
0	0	245 ± 120	0	162 ± 78	0.000	0.960
2.4	< 100	352 ± 194	0	236 ± 110	< 0.008	1.520
24	123 ± 86	335 ± 208	< 100	303 ± 190	0.282	1.680
240	163 ± 113	520 ± 334	< 100	577 ± 356	0.745	1.280

had exhibited a similar creep rate to the 240 h annealed specimen up to ~500 h transitioned to tertiary creep soon after 500 h and failed at a little over 600 h.

After solutionizing Fe-20Cr-30Ni-2 Nb-5Al at 1250 °C, annealing at 800 °C produces both B2 NiAl and Laves phase precipitates. The $L1_2$ precipitates are not stable at that temperature, as detailed in our previous precipitation studies [23,24]. However, they are stable at 760 °C. Thus, TEM examination was performed on each of the heat-treated alloys to examine the sizes of the resulting $L1_2$ precipitates after the 500 h creep tests. Fig. 6 shows typical images after 0 h and 2.4 h in which spherical $L1_2$ precipitates can be observed. The accompanying selected area diffraction pattern shows superlattice reflections consistent with a $L1_2$ crystal structure. The $L1_2$ particle sizes after the 24 h and 240 h appear to be slightly larger at 53–54 nm than those (43–44 nm) after the 0 h or 2.4 h anneals, although for the 0 and 24 h anneal the difference is within the measurement error, as shown in Table 4. Table 4 also shows the volume fraction of $L1_2$ particles, which appears to show an increase with increase in annealing time at 800 °C. Given the slightly larger particles and larger volume fractions at longer annealing times, which means smaller interparticle spacings, one might expect that the samples given longer anneals would creep more slowly. This is the opposite of the observed behavior, suggesting that the $L1_2$ precipitate do not greatly affect the strength. Thus, the differences in creep rates must be due to the NiAl and Laves phase precipitates.

Figs. 7–9 are BSE images of solutionized Fe-20Cr-30Ni-2 Nb-5Al specimens given different heat treatments at 800 °C before and after creep testing. For the solutionized only specimen no precipitates were present before creep testing while both Laves phase and NiAl precipitates are evident after creep testing (Fig. 7). As noted above $L1_2$ precipitates also form during creep testing in this specimen. For specimens given heat treatments at 800 °C prior to creep testing, it is evident that the Laves phase and NiAl precipitates in the matrix coarsen during creep testing. Table 5 lists the sizes of the NiAl and Laves phases in the matrix before and after creep testing along with particle density. The area fraction of grain boundary Fe_2Nb Laves phase and NiAl precipitates increased with aging time, see Table 6. When the sample was fully solutionized at 1250 °C, there was no grain boundary coverage by precipitates. After aging for 2.4 h at 800 °C, the grain boundary area fraction was 42% with only the Laves phase on the grain boundaries. The grain boundary coverage was 69% for samples aged for 24 h and increased to 77% for samples aged 240 h, with both NiAl and Laves phase precipitates on the grain boundaries.

4. Discussion

In contrast to previous studies on AFA steels, the creep properties of Fe-20Cr-30Ni-2 Nb-5Al at 760 °C correlate well with yield stress determined at a strain rate of 5×10^{-4} s^{-1} at the same temperature. The specimens with the finest NiAl and Laves phase particles which were < 100 nm prior to creep testing (annealed 2.4 h at 800 °C) showed the highest yield strength. Note that for all heat treatments, the $L1_2$ were not present at the start of the creep tests but they nucleated and grew throughout the tests. The $L1_2$ particle sizes after 500 h were, within measurement error, the same for all heat treatments. Thus, while the $L1_2$ particles presumably affected the creep rate, this was similar for all heat treatments. Interestingly, the creep rates of the 2.4 h and 24 h annealed specimens show similar creep rates but the 24 h annealed specimen showed greater creep strain after 500 h because of the larger strain acquired in primary creep. The matrix particle sizes for these two specimens are fairly similar but the grain boundary coverage by particles is much greater (69%) for the 24 h annealed compared to the 2.4 h annealed sample (42%). This suggests that the grain boundary precipitates have little influence on the creep rate or alternatively, 42% grain boundary coverage prevents grain boundary sliding and grain boundary coverage greater than this value makes little difference.

The post-creep specimens (Figs. 7–9) did not show signs of grain

Table 6
Area fraction of grain boundary (GB) Laves phase and NiAl precipitates for Fe-20Cr-30Ni-2 Nb-5Al (at%) homogenized at 1250 °C and aged at 800 °C for 0, 2.4, 24 or 240 h. The GB area fraction is calculated from an average of three BSE images for each aging condition.

Aging Time (h)	GB area Fraction (%)
0	0
2.4	42
24	69
240	77

boundary fracture or fracture of the Laves phase precipitates. Both grain boundary fracture and fracture of the Laves phase precipitates has been observed after creep testing an AFA stainless steel with a more complex chemistry [35]. In that case, tests were performed under higher loads (100 MPa and 156 MPa) to fracture, which took over 5000 h. It is worth noting that the Laves phase particles that fractured in those studies were ones present from casting which weren't solutionized upon annealing at elevated temperature. Note that at 700 °C the Laves phase precipitates in AFA steels have been shown to undergo plastic deformation [11].

A surprising feature of all the creep curves for tests up to 500 h is that the creep rates seem constant for a particular heat treatment even though the sizes of the $L1_2$, NiAl and Laves phase precipitates increase during the creep testing. Future work will examine how the particles evolve as a function of time.

5. Conclusions

A correlation between the creep rate and yield strength at 760 °C of heat treated Fe-20Cr-30Ni-2 Nb-5Al was observed with specimens containing the finest initial Laves phase and NiAl particle size showing the highest yield strength and smallest creep strain. Thus, contrary to previous suggestions [2,8], the NiAl and Laves phase particles clearly affect the creep strength. The $L1_2$ particles precipitated out during creep testing, but they do not appear to have greatly affected the creep behavior. The extent of grain boundary coverage by the NiAl and Laves phase precipitates also did not appear to affect the creep rates.

Acknowledgments

This research was supported by National Science Foundation (NSF) Grants DMR 1206240 and DMR 1708091. Any opinions, findings, and conclusions or recommendations expressed in this material are those of the author(s) and do not necessarily reflect the views of the NSF. The use of the Dartmouth Electron Microscope Facility is acknowledged

References

[1] N.P. Afonina, Study of Creep of Alumina-Forming Austenitic Stainless Steel for High-Temperature Energy Applications (M.S. Thesis), Dartmouth College, 2017.
[2] H. Bei, Y. Yamamoto, M.P. Brady, M.L. Santella, Aging effects on the mechanical properties of alumina-forming austenitic stainless steels, Mater. Sci. Eng. A 527 (2010) 2079–2086.
[3] M.P. Brady, C.T. Liu, Y. Yamamoto, Z.P. Lu, H. Meyer Multi-phase high temperature alloys: exploration of Laves phase strengthening of steels, in: Proceedings of the 19th annual conference on fossil energy materials, Knoxville, TN; 9-11th May, 2005. Available at: ⟨www.ornl.gov/sci/fossil/⟩.
[4] M.P. Brady, Y. Yamamoto, M.L. Santella, B.A. Pint, Effects of minor alloy additions and oxidation temperature on protective alumina scale formation in creep-resistant austenitic stainless steels, Scr. Mater. 57 (2007) 1117–1120.
[5] M.P. Brady, Y. Yamamoto, Z.P. Lu, C.T. Liu, P.J. Maziasz, B.A. Pint, Oxidation resistant, high creep strength austenitic stainless steel, US Patent Disclosure; January 4, 2007b.
[6] M. Brady, Y. Yamamoto, M.L. Santella, P. Maziasz, B. Pint, C. Liu, Z. Lu, H. Bei, The development of alumina-forming austenitic stainless steels for high-temperature structural use, JOM J. Miner. Met. Mater. Soc. 60 (2008) 12–18.
[7] M.P. Brady, J. Magee, Y. Yamamoto, D. Helmick, L. Wang, Co-optimization of wrought alumina-forming austenitic stainless steel composition ranges for high-temperature creep and oxidation/corrosion resistance, Mater. Sci. Eng.: A 590 (2014) 101–115.
[8] X. Dong, L. Zhao, F. Sun, L. Zhang Strengthening of an Al-containing austenitic stainless steel at high temperature, in: Proceedings of ASME Turbo Expo 2013: Turbine Technical Conference and Exhibition (GT2013), San Antonio, TX, 3-7 June 2013.
[9] F. Garofalo, O. Richmond, W.F. Domis, Design of apparatus for constant-stress or constant-load creep tests, J. Basic Eng. 84 (1962) 287–293.
[10] U. Heubner, Nickel Alloys, CRC Press, 2000.
[11] B. Hu, I. Baker, High temperature deformation of laves phase precipitates in alumina-forming austenitic stainless steels, Mater. Lett. 195 (2017) 108–111.
[12] P. Kofstad, Defects and transport properties of metal oxides, Oxid. Met. 44 (1995) 3–27.
[13] P.J. Maziasz, Developing an austenitic stainless-steel for improved performance in advanced fossil power facilities, J. Met. 41 (1989) 14–20.
[14] J.A. McGurty, Austenitic Iron Alloys, US Patent No. 4,086,085, April 1978, 1978.
[15] M.K. Miller, D.T. Hoelzer, E.A. Kenik, K.F. Russell, Stability of ferritic MA/ODS alloys at high temperatures, Intermetallics 13 (2005) 387–392.
[16] M.K. Miller, E.A. Kenik, K.F. Russell, L. Heatherly, D.T. Hoelzer, P.J. Maziasz, Atom probe tomography of nanoscale particles in ODS ferritic alloys", Mater. Sci. Eng. A353 (2003) 140–145.
[17] G. Smith, L. Shoemaker Advanced nickel alloys for coal-fired boiler tubing, Advanced Materials and Processes, 162: 23-26.
[18] M. Takeyama, Novel concept of austenitic heat resistant steels strengthened by intermetallics, Mater. Sci. Forum 539–543 (2007) 3012–3017.
[19] M. Takeyama, S. Morita, A. Yamauchi, M. Yamanaka, T. Matsuo Phase MatsuoEquilibria among γ, Ni_3Nb-δ and Fe_2Nb-ε phases in Ni-Nb-Fe and Ni-Nb-Fe-Cr. Systems at Elevated Temperatures, in: Loria E.A. , editor. Superalloys 718, 625, 706 and various derivatives. TMS, p. 333-344.
[20] I. Tarigan, N. Takata, T. Matsuo, M. Takeyama, Novel concept of creep strengthening mechanism using grain boundary Fe_2Nb laves phase in austenitic heat resistant steel, MRS Proc. 1295 (2011) 317–322.
[21] I. Tarigan, N. Takata, Y. Terada, M. Takeyama, Grain Boundary Precipitation Strengthening Mechanism by Fe_2Nb Laves Phase in Creep of Fe-20Cr-30Ni-2Nb Austenitic Heat-Resistant Steel, in: Proceedings of the 12th International Conference on Creep and Fracture of Engineering Materials and Structures (JIMIS 11) Kyoto, Japan, The Japan Institute of Metals, May 27-31, 2012, 2012.
[22] G. Trotter, I. Baker, The effect of aging on the microstructure and mechanical behavior of the alumina-forming austenitic stainless steel Fe-20Cr-30Ni-2Nb-5Al, Mater. Sci. Eng. A 627 (2015) 270–276.
[23] G. Trotter, I. Baker, Orientation relationships of laves phase and NiAl particles in an AFA stainless steel, Philos. Mag. 95 (2015) 4078–4094.
[24] G. Trotter, G. Rayner, I. Baker, P.R. Munroe, Accelerated precipitation in the AFA stainless steel Fe-20Cr-40Ni-2Nb-5Al via cold working, Intermetallics 53 (2014) 120–128.
[25] G. Trotter, B. Hu, Annie Y. Sun, R. Harder, M.K. Miller, L. Yao, I. Baker, Precipitation kinetics during aging of an alumina-forming austenitic stainless steel, Mater. Sci. Eng. 667 (2016) 147–155.
[26] R. Viswanathan, W.T. Bakker, Materials for Boilers in Ultra supercritical power plants, in: Proceedings of 2000 International Joint Power Generation Conference Miami Beach, Florida, July 23-26, p1-p22, 2000.
[27] R. Viswanathan, J.F. Henry, J. Tanzosh, G. Stanko, J. Shingledecker, B. Vitalis, R. Purgert, U.S. program on materials technology for ultra-supercritical coal power plants, J. Mater. Eng. Perform. 14 (2005) 281–292.
[28] Y. Yamamoto, M.P. Brady, Z.P. Lu, P.J. Maziasz, C.T. Liu, B.A. Pint, Creep-resistant, Al_2O_3-forming austenitic stainless steels, Science 316 (2007) 433–436.
[29] Y. Yamamoto, M.P. Brady, Z.P. Lu, C.T. Liu, M. Takeyama, P.J. Maziasz, et al., Alumina-forming austenitic stainless steels strengthened by Laves phase and MC carbide precipitates, Metall. Mater. Trans. A 38A (2007) 2737–2746.
[30] Y. Yamamoto, Z.P. Lu, M.P. Brady, C.T. Liu, P.F. Tortorelli Multi-phase high temperature alloys: exploration of Laves phase strengthening of steels, in: Proceedings of the 20th annual conference on fossil energy materials. Knoxville, TN; 9-11th May, 2005. Available at: ⟨www.ornl.gov/sci/fossil/⟩.
[31] Y. Yamamoto, M. Takeyama, Z.P. Lu, C.T. Liu, N.D. Evans, P.J. Maziasz, M.P. Brady, Alloying effects on creep and oxidation resistance of austenitic stainless steel alloys employing intermetallic precipitates, Intermetallics 16 (2008) 453–462.
[32] Y. Yamamoto, M.L. Santella, M.P. Brady, H. Bei, P.J. Maziasz, Effect of alloying additions on phase equilibria and creep resistance of alumina-forming austenitic stainless steels, Metall. Mater. Trans. 40A (2009) 1868–1880.
[33] Y. Yamamoto, M.P. Brady, M.L. Santella, P.J. Maziasz, B.A. Pint, Overview of strategies for high-temperature creep and oxidation resistance of alumina-forming austenitic stainless steels, Metall. Mater. Trans. 42A (2011) 922–931.
[34] Y. Yamamoto, G. Muralidharan, M.P. Brady, Development of $L1_2$-ordered $Ni_3(Al,Ti)$ strengthened alumina-forming austenitic stainless steel alloys, Scr. Mater. 69 (2013) 816–819.
[35] B. Hu, I. Baker, S.J. Kernion, Y. Yamamoto and M.P. Brady, Eighth International Conference on Advances in Materials Technology for Fossil Power Plants, Algarve, Portugal, October 10-14, 2016, p.295-303.